Quantum cascade lasers grown by MOCVD

Yongqiang Sun[1, 2, 3], Guangzhou Cui[1, 2, 3], Kai Guo[1, 2], Jinchuan Zhang[1, 2, †], Ning Zhuo[1, 2], Lijun Wang[1, 2, 3], Shuman Liu[1, 2, 3], Zhiwei Jia[1, 2], Teng Fei[1, 2, 3], Kun Li[1, 2, 3], Junqi Liu[1, 2, 3], Fengqi Liu[1, 2, 3], and Shenqiang Zhai[1, 2, †]

[1]Key Laboratory of Semiconductor Materials Science, Institute of Semiconductors, Beijing100083, China

[2]Beijing Key Laboratory of Low Dimensional Semiconductor Materials and Devices, Beijing100083, China

[3]Center of Materials Science and Optoelectronics Engineering, University of Chinese Academy of Sciences, Beijing 100049, China

Abstract: Sharing the advantages of high optical power, high efficiency and design flexibility in a compact size, quantum cascade lasers (QCLs) are excellent mid-to-far infrared laser sources for gas sensing, infrared spectroscopic, medical diagnosis, and defense applications. Metalorganic chemical vapor deposition (MOCVD) is an important technology for growing high quality semiconductor materials, and has achieved great success in the semiconductor industry due to its advantages of high efficiency, short maintenance cycles, and high stability and repeatability. The utilization of MOCVD for the growth of QCL materials holds a significant meaning for promoting the large batch production and industrial application of QCL devices. This review summarizes the recent progress of QCLs grown by MOCVD. Material quality and the structure design together determine the device performance. Research progress on the performance improvement of MOCVD-grown QCLs based on the optimization of material quality and active region structure are mainly reviewed.

Key words: quantum cascade lasers; continuous wave; high optical power; metal organic chemical vapor deposition; broad gain

1. Introduction

The quantum cascade laser (QCL)[1], which operates based on sub-band transitions, is an ideal source for mid-to-far infrared radiation. Sharing the advantages of high efficiency, high optical power, and design flexibility in a compact size, QCLs are excellent laser sources in numerous application fields, such as gas sensing[2–5], infrared spectroscopy[6, 7], medical diagnosis[8] and defense applications[9, 10]. The QCL materials typically consist of hundreds of alternating and coupled nanoscale thin InGaAs/InAlAs layers[11], as depicted in Fig. 1, and material quality and the structure design together determine device performance. Since the original implementation of QCLs in 1994, extensive research on material structure design and epitaxial growth has been done. In terms of material growth, molecular beam epitaxy (MBE) has the natural advantage in preparing QCLs due to its ability to precisely control growth parameters and create steep interfaces. Therefore, MBE technology has been predominantly used for material preparation during the development of QCL technology. Bai *et al.* obtained a continuous wave (CW) room temperature output power of 5.1 W with lasering wavelength of 4.9 *μ*m based on MBE[12], which is the highest output power of standard single ridge QCL devices at present. However, the MBE technique because of ultra-high vacuum operating processes result in low production efficiency and high costs for widespread implementation of QCLs.

Metalorganic chemical vapor deposition (MOCVD) is another competitive counterpart technique for growth of high-quality semiconductor materials. Due to the advantages of high efficiency, short maintenance cycles, and high stability and repeatability, MOCVD has achieved great success in the semiconductor industry. To promote the industrial production of QCLs, growth of QCLs using MOCVD has thus drawn great interest. However, there are tricky challenges in the growth of QCL materials based on MOCVD to obtain high performance. Due to the long source pipeline, when the corresponding pneumatic valve is turned off, the source flow cannot turn to zero suddenly because of the source material residual. This will result in element mixing at the interfaces, which can impact the band structures and thus the device performance. In addition, most high performance QCL material structures are designed and optimized for growth based on MBE. Considering the characteristics of MOCVD-grown materials, specialized structure design and optimization for high performance are necessary. Over the past few decades, considerable efforts have been made to overcome the challenges mentioned above and a lot of high-performance room temperature CW QCLs grown by MOCVD have been reported. In 2003, the first MOCVD-grown QCL was demonstrated based on GaAs substrate[13], and subsequently room temperature operation was realized based on InP/InGaAs/InAlAs material system[14] in the same year. In 2006, QCLs grown by MOCVD[15, 16] demonstrated comparable performance to their early MBE-grown counterparts[17]. In both mid- and far-infrared wavelength range, CW output powers at room temperatures exceeding watt level have been achieved[18–24]. In particular, fully taking the advantage of the growth flexibility of MOCVD, Botez *et al.* designed tapered
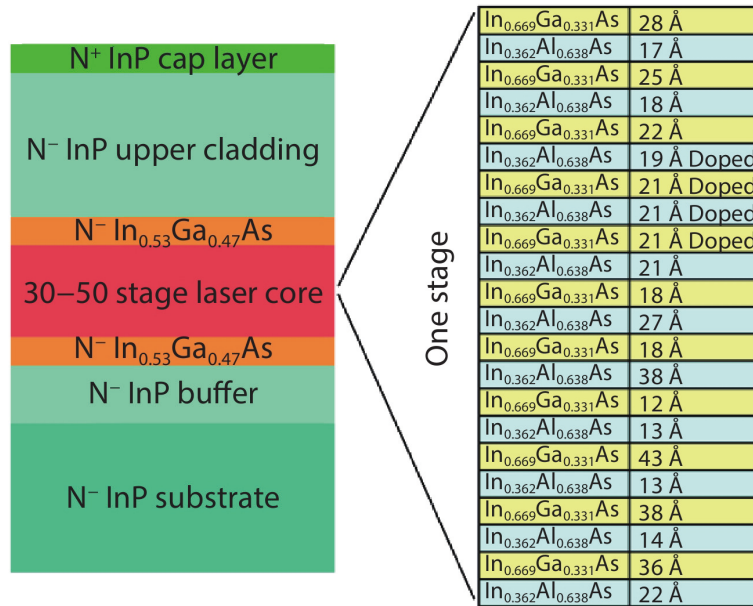
Fig. 1. (Color online) Typical mid infrared QCL structure[11].

active region structures, and a room temperature CW power of 2.6 W at 5 μm was achieved[24, 25]. As the research on MOCVD-grown QCLs moves along, QCL technology is facing a promising opportunity of large-scale production and industry application. In this work, we provide an overview on the recent research of QCLs grown by MOCVD, mainly focusing on the performance improvement of MOCVD-grown QCLs based on the optimization of material quality and the active region structure.

2. Long-wavelength infrared MOCVD-grown QCLs

2.1. Lattice matched MOCVD-grown LWIR QCLs

QCLs operating in the long-wavelength infrared (LWIR) band with low photon energy ($\lambda = 8–12$ μm) typically employ lattice-matched $In_{0.53}Ga_{0.47}As/In_{0.52}Al_{0.48}As$ materials on an InP substrate. The offset band of 520 meV for this material system provides enough energy space for the structure design of LWIR QCLs. Since the growth of lattice matched materials is relatively easy, researchers first tried the growth of LWIR QCLs using MOCVD. Indeed, the first MOCVD-grown QCL was demonstrated based on GaAs/AlGaAs material system on GaAs substrate[13], which is lattice matched naturally. However, due to the large electron effective mass, QCLs based on GaAs substrate get stuck in performance improvement and are gradually abandoned. Subsequently, emitting wavelengths of 7.1[26], 8.5[14] and 9 μm[27] MOCVD-grown QCLs on InP substrates were reported. By utilizing vent/run valves that have been individually purged and maintaining a low growth rate for the active region, the precise control of interfacial sharpness and layer thicknesses was successfully obtained. However, these devices were unable to operate in continuous wave mode at room temperature. Troccoli *et al.* realized the first room temperature CW MOCVD-grown QCL with lasing wavelength of 7.2 μm in 2005[28]. Through further optimization of growth parameters, high-power QCLs with 8.38 μm were presented in CW mode above 400 K[29]. These devices exhibited a maximum continuous wave output power of 204 mW at 300 K, and initial reliability data obtained from accelerated aging tests indicated the remark-

able robustness of these devices.

Next, the performance of MOCVD-grown QCLs were improved gradually through active design optimization. Fujita *et al.* proposed a new QCL structure with single phonon resonance-continuum (SPC) depopulation and room temperature CW operations at 7.9[30] and 8 μm[31] were realized. Fig. 2(a) shows the schematic conduction band diagram of the active region. In this SPC-depopulation design, the lowest states of the active region formed a miniband and the wavefunctions extended over the injector region. Furthermore, the lower lasing level was separated by one phonon energy from the top state of the miniband. These features resulted in high performance, and also allowed for layer-thickness fluctuations. With this design, a 4 mm-long, 8 μm-wide, high reflective (HR)-coated device demonstrated a high output power of 313 mW in CW operation presented in Fig. 2(b). The maximum CW lasing temperature was measured up to 120 °C. Based on active design optimization, Pflugl *et al.* also reported high-power CW operation of 9.5 μm QCLs grown by MOCVD with no less than hundreds of milliwatts at room temperature[32].

The material quality of the epitaxial layer in a QCL has a major impact on device performance. Therefore, it is very meaningful to explore the relationship between epitaxial growth and material properties for continuous improvement of these properties. The impact of growth parameters on material quality has been extensively investigated in the subsequent development of MOCVD-grown QCLs. Huang *et al.* systematically investigated the influence of multiple factors on surface morphology, optical quality, and impurity incorporation. These include growth temperature, substrate misorientation and Ⅴ/Ⅲ ratio[33]. According to their research, epitaxial materials with Ⅴ/Ⅲ ratios of 116 for InGaAs and 21 for InAlAs that were produced at a temperature of 720 °C on InP substrates with an off-cut angle of roughly 0.061 displayed consistent step-flow development and little impurity contamination, as illustrated in Fig. 3. Demir *et al.* reported the effects of interruption time between each layer and Ⅴ/Ⅲ ratio on high quality InAlAs/InGaAs superlattice (SL) structures[34, 35].
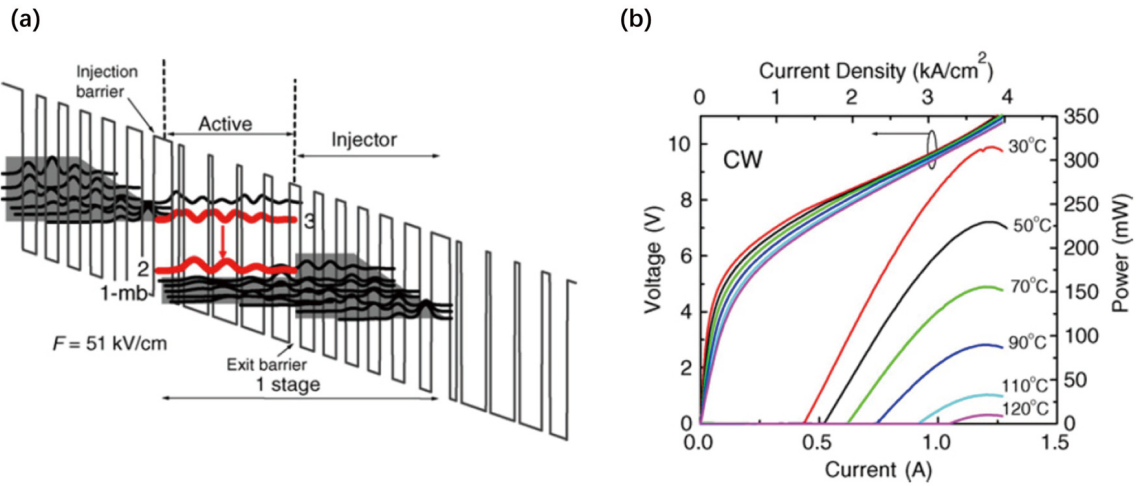
Fig. 2. (Color online) (a) A schematic diagram of the energy band under an electric field intensity of 51 kV/cm. (b) CW P–I–V curves of laser with 8 μm ridge width and 4.0 mm cavity length at different heat sink temperatures[31].
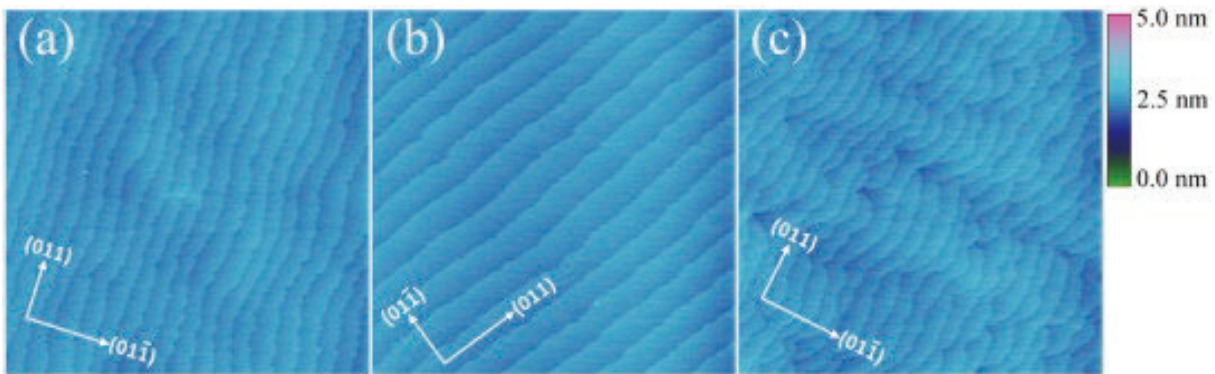

Fig. 3. (Color online) AFM images (10 × 10 μm^2) of 30-period of $In_{0.53}Ga_{0.47}As$/$In_{0.52}Al_{0.48}As$ (8/15 nm) multi-quantum wells (MQWs) grown at (a) 680 °C, (b) 720 °C, and (c) 760 °C. The height scale is 5 nm for all images[33].
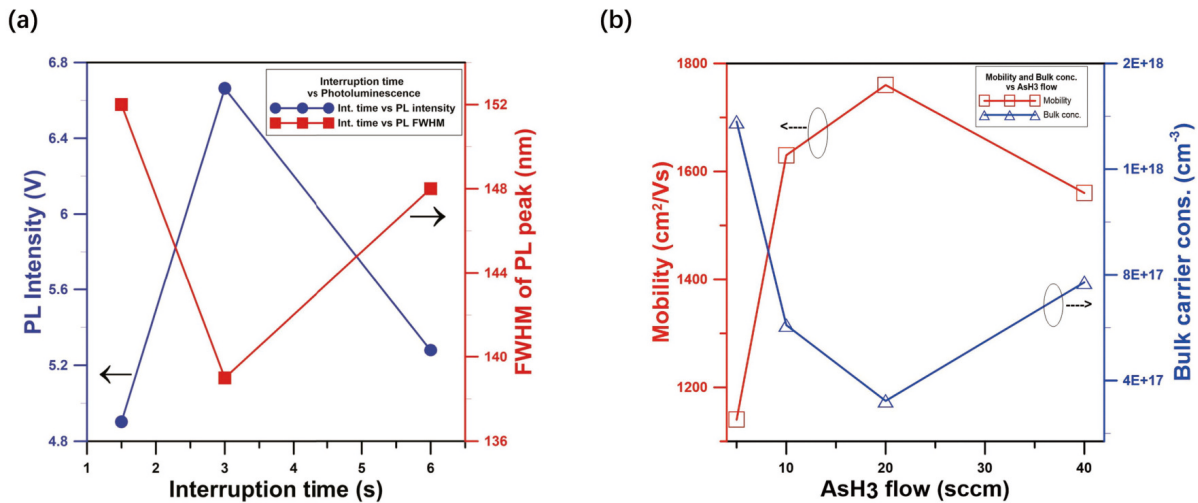

Fig. 4. (Color online) (a) Interruption time versus PL intensity of emission and FWHM of PL peak, (b) mobility and bulk carrier concentration behavior of $In_xAl_{1-x}As$ epilayers with increasing AsH_3 flow from 5 to 40 sccm[34, 35].

The quality of the SLs was significantly improved by introducing interruption delays during the growth, as evidenced by their crystallinity, interface sharpness, and optical properties. The results show that an optimal interruption delay time value could bring in sharper interfaces and improved optical and structural properties[34]. Fig. 4(a) demonstrated obvious improvements of photoluminescence (PL) intensity and the full width at half maximum (FWHM) of PL peak with an interruption time of 3 s. Their study also demonstrated that maintaining a fixed metalorganic precursor flow to achieve an optimal V/III ratio is a critical parameter for ensuring high material quality in $In_xAl_{1-x}As$ layers[35]. These studies provide useful references for the growth of high-quality QCL materials based on MOCVD for other researchers.

Table 1. Details of nominally lattice-matched AlInAs/GaInAs superlattice structures and $n = 0$ peaks obtained through high-resolution X-ray diffraction measurement. SLs were grown without growth interruption, except for samples with *, where the interruption time was 4 s after barrier and well layer growth[36].

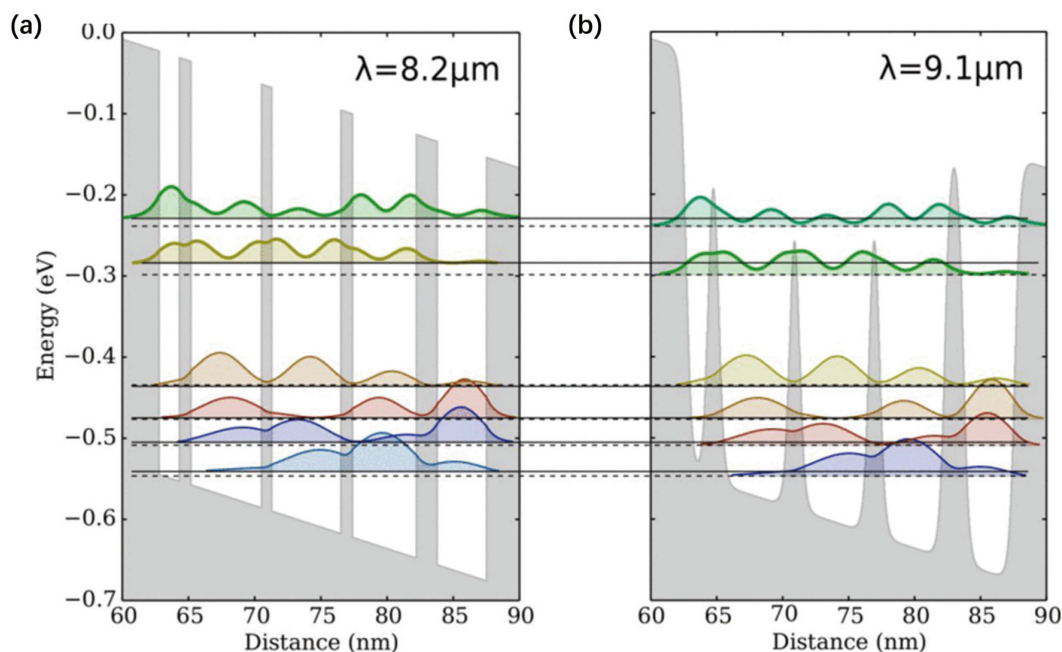| Sample	Barrier thickness (nm)	Well thickness (nm)	SL period	Number of periods	$n = 0$ peak position (rel arcs)
1123	10	10	20	20	−10
1124*	10	10	20	20	−18
1125	10	2.5	12.5	32	−107
1126	2.5	10	12.5	32	−104
1127	5	5	10	40	−134
1128	2.5	2.5	5	80	−335
1129*	2.5	2.5	5	80	−315

Fig. 5. (Color online) Calculated conduction band diagram of (a) the abrupt interface (8.2 μm) in the active region of the QCL, (b) the gradient interface (9.1 μm) in the active region of the QCL[23].
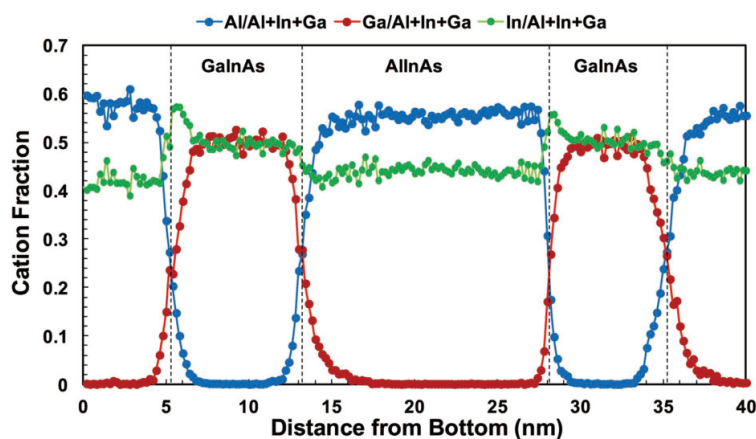

Fig. 6. (Color online) Cation concentration profiles of Al, Ga, and In in AlInAs/GaInAs MQWs. The growth direction is from left to right. The blue, red, and green curves, respectively, represent the composition contents of Al, Ga, and In in the MQWs[37].

Wang *et al*. systematically studied composition profile at the interfaces from the microscopic atomic scale and demonstrated their effects on lasering wavelengths and device performance[23, 36, 37]. Systematic $n = 0$ peak shifts were observed in high-resolution X-ray diffraction measurements as the AlInAs/GaInAs layers decreased below approximately 10 nm

in nominally lattice-matched AlInAs/GaInAs superlattices, as presented in Table 1[36]. They attributed this shift to indium surface segregation in both InAlAs and InGaAs. These shifts were specifically compensated for through fine-tuning the precursor flow and devices resulting in a peak power of 5.3 W emitted from one side at 20 °C. They have also elucidated the red-
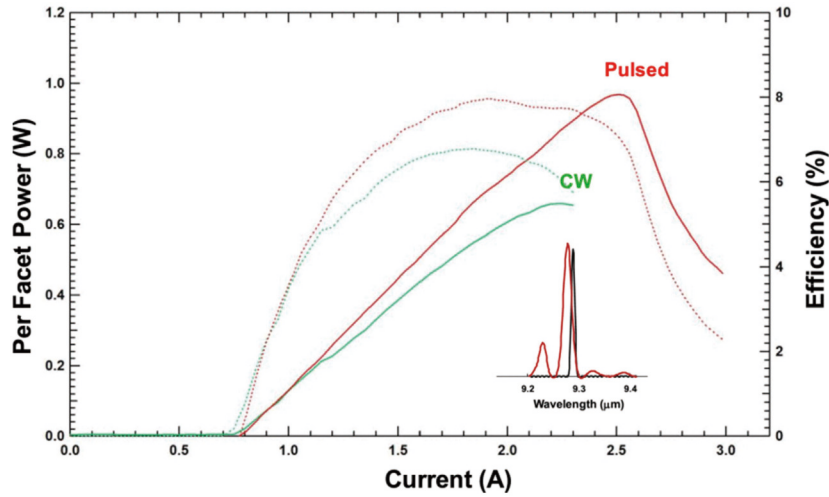
Fig. 7. (Color online) Curves of pulsed and continuous wave operation of a 9.3 μm uncoated buried heterostructure QCL (12 μm × 5 mm long) measured at 15 °C[23].
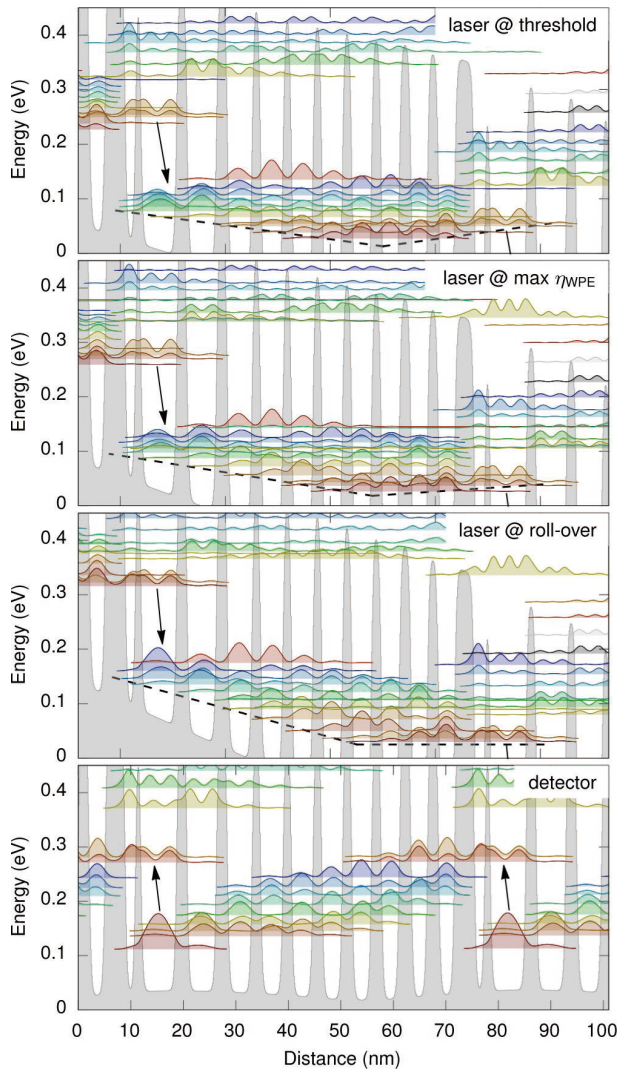

Fig. 8. (Color online) Energy band diagrams at the laser threshold, the bias with the highest pulsed electrical insertion efficiency, flip bias, and detector bias (zero bias)[39].

Fig. 9. (Color online) Calculated energy diagram of a QCL based on a $Ga_{0.47}In_{0.53}As/Al_{0.48}In_{0.52}As$ heteropair. The intensity of the applied electric field is 62 kV/cm[40].

shift in lasing wavelength observed in MOCVD-grown QCLs, which refers to a reported phenomenon of these QCLs lasing at wavelengths 0.5−1 μm longer than their intended design[37]. This study revealed that the InAlAs/InGaAs heteroint-
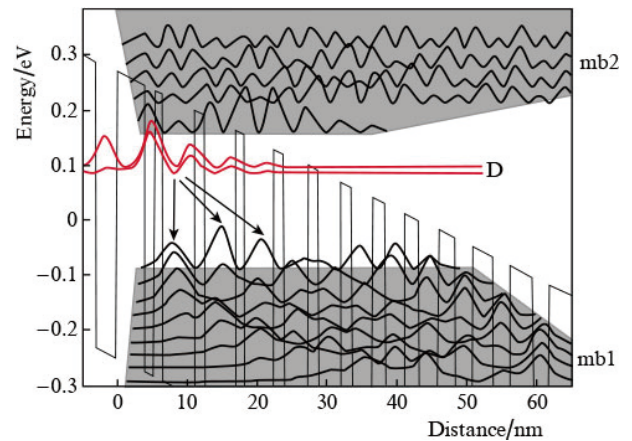
erfaces exhibited a compositional gradient spanning 2.5−4.5 nm, indicating that the as-grown QCLs did not possess the ideal abrupt interfaces utilized in QCL modeling. This deviation of interface morphology resulted in the wavelength red shifts, as shown in Fig. 5. To further study the details of the interface topography, the cation distribution was measured by atom probe tomography (APT), and the results are shown in Fig. 6[37]. APT is a nano-characterization technique capable of mapping chemical composition at the atomic spatial scale, which is a powerful tool for studying the characteristics of ultra-thin semiconductor materials[38]. The results indicated that the heterointerface exhibited a compositional gradient, with an excess of indium at the InAlAs-to-InGaAs interface. Additionally, it was discovered that the barrier layer consists of an AlGaInAs quaternary system rather than AllnAs, and its aluminum content decreased[37]. To rectify the composition, a secondary flow of Al precursor was introduced during growth to increase the Al content, which would result in a reduction of emission wavelength. Based on this research, growth parameters were optimized, and 9.3-μm MOCVD-grown QCLs with CW output power of 1.32 W and maximum WPE of 6.8% were demonstrated, as shown in Fig. 7[23]. This WPE was more than 50% greater than previ-
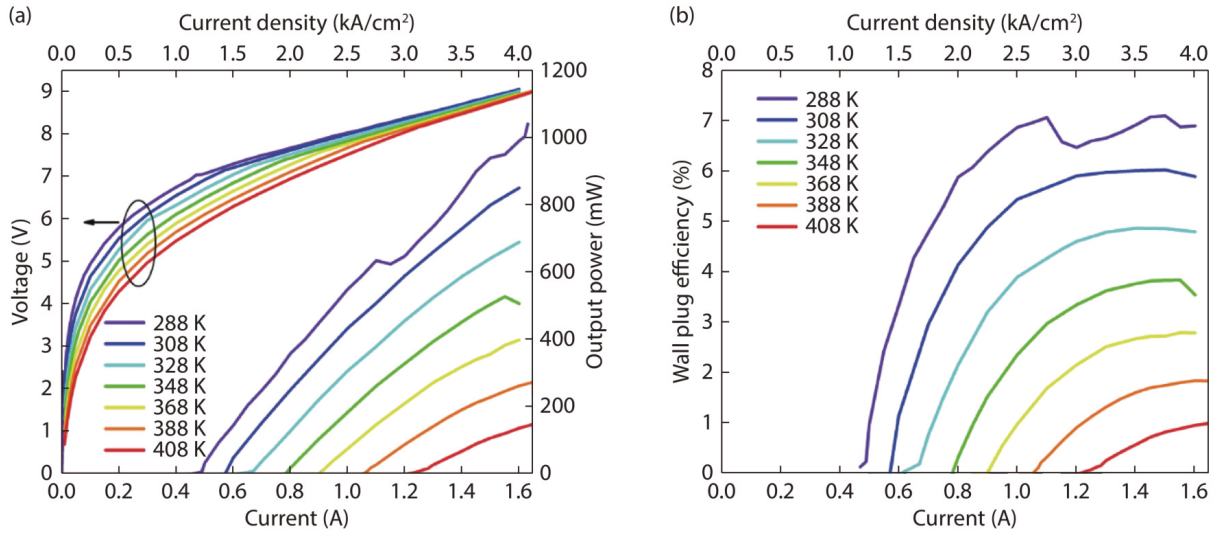
Fig. 10. (Color online) *P–I–V* of a 10 *µ*m × 4 mm long, HR-coated laser under CW conditions at different temperatures. (b) Variation curves of WPE with current injection at different temperatures[42].
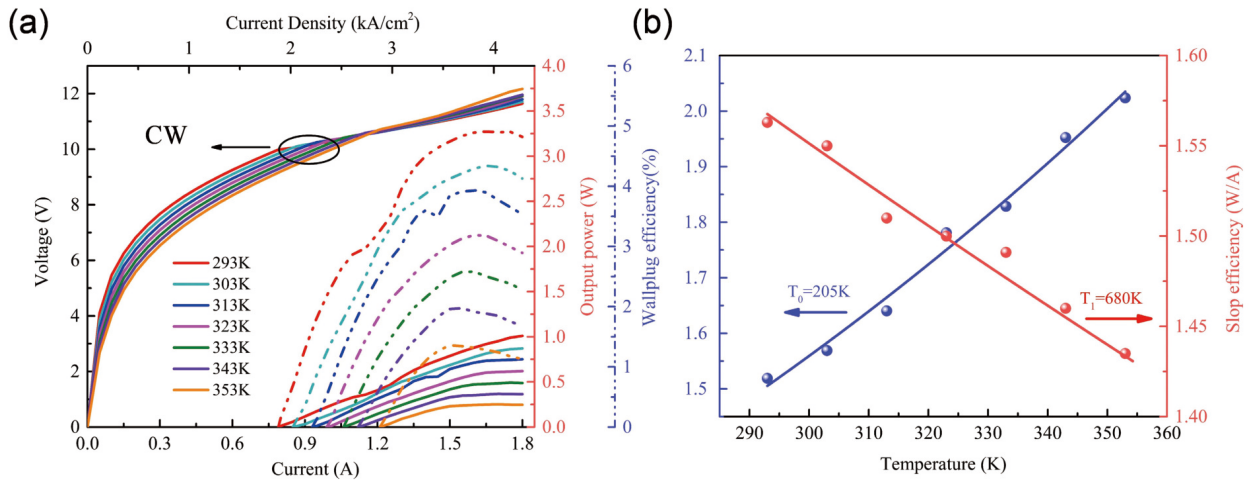

Fig. 11. (Color online) (a) The right-hand colored solid line represents the power curve, and the right-hand colored dashed line represents the WPE curve. (b) The mid-threshold current density and the slope efficiency near the threshold under the operation of pulse operation (480 ns, 20 kHz) vary with the temperature of the heat sink changing characteristics[19].

ously reported WPEs for lattice matched QCLs emitting at 8.9 *µ*m. This research provided great guidance for the optimization of growth parameters and band structure design.

Numerous groups have pursued MOCVD for lattice matched LWIR QCLs, and have achieved a high level of success. A 8.5 *µ*m MOCVD-grown bi-functional QC laser/detector was demonstrated by Schwarz *et al.*, as shown in Fig. 8[39]. As a laser, a WPE of 7% and a maximum power output of 1.05 W in CW mode were obtained. The bi-functional structures, capable of light emission and detection at the same wavelength, allowed the realization of the integrated mid-infrared photonics for sensing applications. Molodtsov *et al.* developed a high temperature operation QCL emitting at a wavelength of 7.4 *µ*m, as shown in Fig. 9. In a pulse mode, the maximal operation temperature was up to 371 K. Such a high temperature can be explained by two factors: a large energy of the transfer from the doublet to the upper miniband and a large volt defect[40]. Recently, Fei *et al.* reported a 8.5 *µ*m MOCVD-grown QCL with an impressive WPE of 7.1% and CW output power of 1.04 W at 288 K, as shown in Fig. 10. It is important to point out that this device also showed excel-

lent temperature stability. Threshold-current characteristic temperature coefficient T_0 of 228 K, and slope-efficiency characteristic temperature coefficient T_1 of 680 K were obtained, as shown in Fig. 11(b). The interface roughness (IFR) is an important factor that affects device temperature characteristics because the IFR scattering induced thermally activated current leakage will be enlarged with increasing operating temperatures[19]. Therefore, these excellent temperature characteristics implied that high quality material with reduced IFR were obtained. For wavelengths $\lambda > 10$ *µ*m, MOCVD-grown QCLs based on lattice matched materials also demonstrate some impressive results. Moreau *et al.* reported the pulsed operation of long-wavelength (~11.3 *µ*m) MOCVD-grown QCLs[28]. The peak output power at 77 K was approximately 315 mW, and the devices displayed laser operation up to 350 K. Fan *et al.* reported QCLs designed to emit at 19 *µ*m grown by MOCVD. Their devices were demonstrated to operate in pulsed mode up to 170 K[41]. One of the factors affecting the output power based on LWIR QCLs may be the high intrinsic background doping concentration of InP and GaAs systems. MOCVD is not a high vacuum device. The vacuum degree of
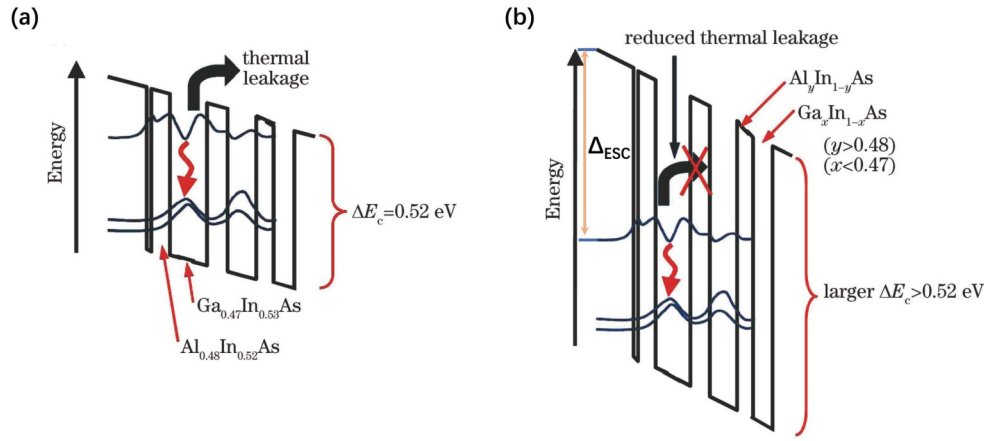
Fig. 12. (Color online) (a) The material $In_{0.52}Al_{0.48}As/In_{0.53}Ga_{0.47}As$ that matches the lattice parameter of InP has $\Delta E_C = 520$ meV; (b) strain compensated $In_{1-x}GaxAs/In_{1-y}Al_yAs$ material on InP with $\Delta E_C > 520$ meV, where $x > 0.53$ and $y < 0.52$.
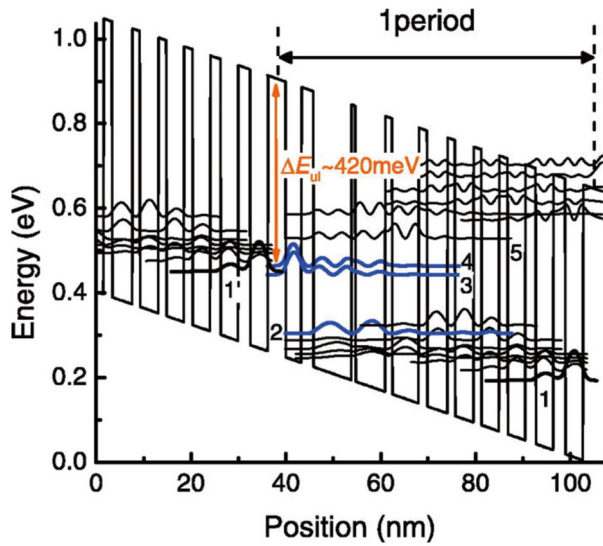

Fig. 13. (Color online) A schematic diagram of the energy band under an electric field intensity of 41 kV/cm[43].

MOCVD is far from reaching the vacuum degree of MBE. This causes a high concentration of background doping.

2.2. Strain-compensated MOCVD-grown LWIR QCLs

Although the growth of lattice-matched InGaAs/InAlAs on InP substrate has small difficulty, the band shift of 520 meV is somewhat too small to further improves device performance, as presented in Fig. 12(a). This happens because this relatively small band shift will result in small energy difference between the upper lasing level and corresponding thermal escaping levels, and thus serious thermal escaping of electrons. Strain-compensated $In_xGa_{1-x}As/In_yAl_{1-y}As$ material system, where $x > 0.53$ and $y < 0.52$, can provide larger band shift and greater potential for performance enhancement. As shown in Fig. 12(b), larger band offset ΔE_c will result in larger Δ_{esc} and thus suppressed carrier leakage. Fujita *et al.* chose strain-compensated $In_{0.6}Ga_{0.4}As/In_{0.44}Al_{0.56}As$ layers to improve the confinement of the electrons of the upper laser states for emitting at 8.5 μm with an anticrossed dual-upper (DAU) design. The conduction-band diagram of injector-active-injector parts is shown in Fig. 13. In this design, another upper laser state was incorporated by the thin quantum well adjacent to the injection barrier. This

thin quantum well reduced the coupling between the miniband states in the injector and higher lying states and played a crucial role for high device performance. Based on this design, the MOCVD-grown lasers exhibited an extremely high characteristic temperature for the threshold current density above 330 K ($T_0 = \sim 750$ K), as shown in Fig. 14. With strain-compensated $In_{0.63}Ga_{0.37}As/In_{0.36}Al_{0.64}As$ materials, Xie *et al.* demonstrated an optimized MOCVD-grown QCL emitting at $\lambda > 10$ μm, which combined the designs of two-phonon resonant and diagonal transitions[20]. The high proportion of Al composition leads to a high barrier, which was beneficial to suppress the leakage of carriers across the barrier at high temperatures. In addition, compared with vertical transitions, diagonal transitions increased the lifetime of electrons on the upper lasing level, resulting in higher efficiency of population inversion. As shown in Fig. 15, a maximum CW output power of 1.3 W was achieved, which demonstrated an encouraging result for the MOCVD-grown LWIR QCLs. Recently, Sun *et al.* also demonstrated a high performance MOCVD-grown QCL based on strained-compensated material with a CW output power of 1.02 W at 293 K[19], as presented in Fig. 11(a).

The active region designs of QCLs have undergone evolution over time, and each major performance improvement always relied on structure design innovations. Compared with MBE, MOCVD has obvious advantages in fast changing material composition during one growth process, due to the fast adjustment capability of precursor flow. This makes it possible to grow SL structures composed of multiple alloy compositions and provides more freedom for material design. From this, a novel QCL structure, namely the step-taper active-region (STA) design, was demonstrated by Botez *et al.*, which consisted of multiple different components $In_xGa_{1-x}As$ and $In_yAl_{1-y}As$[44]. Fig. 16(a) depicts a conventional active region structure design for LWIR (8–9 μm) QCL[45]. Due to the proximity of energy E_5 and E_4 (energy difference ~57 meV), large carrier leakage was expected, which decreased the device performance. For the STA design, the barriers were stepwise tapered, in which the first two barriers were $In_{0.49}Al_{0.51}As$ layers and the third and exit barriers were taller $In_{0.42}Al_{0.58}As$ layers. This step-tapered design caused both a high E_{54} value ~76 meV, as well as a significant decrease in the spatial overlap between levels 5 and 4. This resulted in a high carrier life-
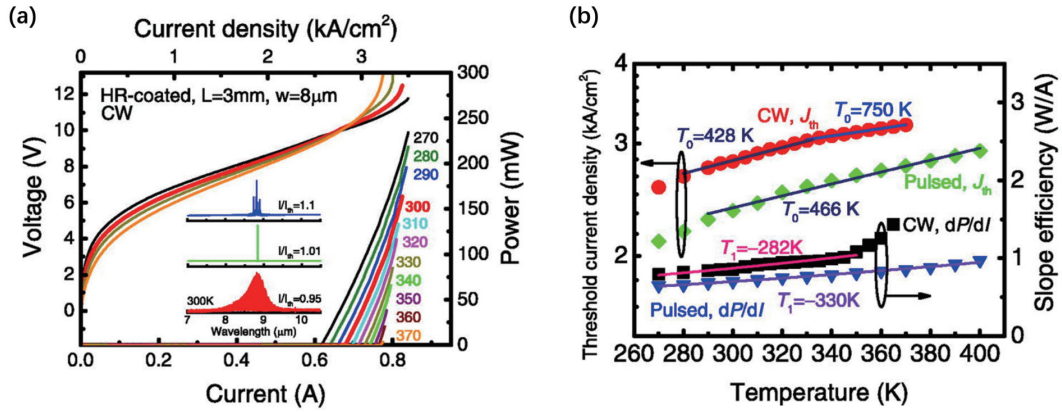
Fig. 14. (Color online) P–I–V of a 8 μm × 3 mm long, HR-coated laser under CW conditions at different temperatures. The inset depicts the spectra of the DAU operating both below and above threshold at a temperature of 300 K. (b) The mid-threshold current density and the slope efficiency near the threshold under the operation of CW operation vary with the temperature of the heat sink changing characteristics[43].
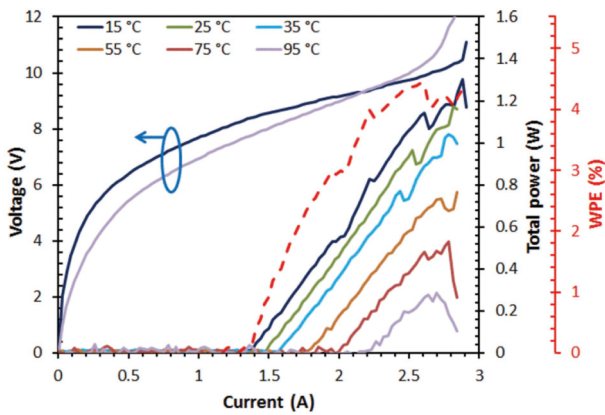

Fig. 15. (Color online) CW (solid line) LIV curves of a laser chip with 11.5 μm wide stripes and 6 mm cavity length from 15 to 95 °C. The dashed red line is the WPE curve at 15 °C[20].

time τ_{45} of 14.7 ps, which was more than four times the value for the conventional QCL (3.6 ps). This device achieved up to 1 W single-sided CW power at a heat sink temperature of 14 °C, as shown in Fig. 17. Then, Botez et al. have in further optimized the STA design with a more complex structure[46]. In this structure, the barrier heights increased stepwise in the active region: x = 0.51, 0.51, 0.58 and 0.58 in In$_{1-x}$Al$_x$As, and the wells depths increased stepwise: x = 0.56, 0.56, 0.61 and 0.62 in In$_x$Ga$_{1-x}$As depicted in Fig. 16(b). Due to the significant suppression of carrier leakage, the device exhibited much higher T_0 and T_1 values compared to conventional 8−9 μm emitting QCLs with similar injector doping levels. It is worth noting that the device demonstrated a high internal quantum efficiency η_i up to 86%, which demonstrated that the STA design has great potential for future laser developments. However, the growth of high-quality materials with such complex structures is a challenge to be overcomed.

3. MOCVD-grown mid-infrared QCLs (3−5 μm)

The mid-infrared wavelength range corresponds to the important atmospheric windows of 3−5 μm. Driven by the urgent demand of optical countermeasures, QCLs in this wavelength range have realized great success and presents higher output power than those in the LWIR range. Based the good research foundation and superior structure designs in this
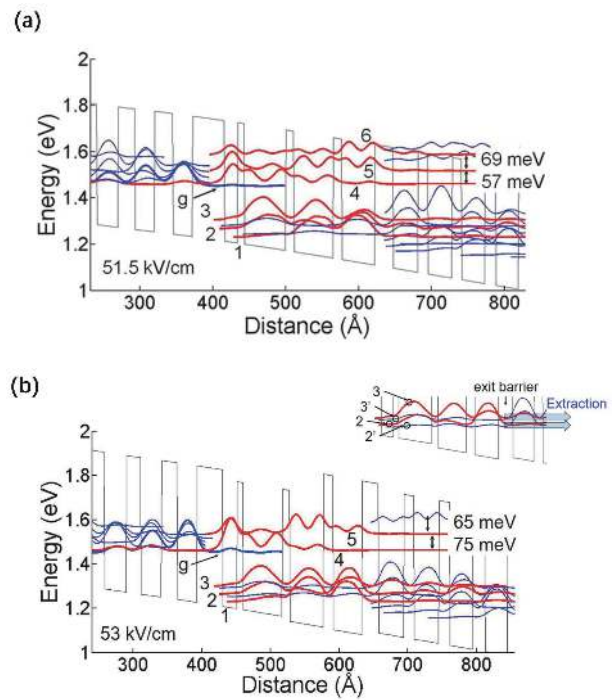

Fig. 16. (Color online) (a) Schematic band diagram and wavefunctions, at threshold, for conventional 8–9 μm QCL[45]. (b) Conduction-band diagram and relevant wavefunctions, at threshold, for the STA QCL[46].

wavelength range, mid-infrared MOCVD-grown QCLs have experienced rapid development. Originally, Diehl et al. reported the room temperature operation of mid-infrared MOCVD-grown QCLs in 2006[15, 29]. They demonstrated devices worked in pulsed mode above 320 K and in CW mode up to 280 K[15]. They then demonstrated 5.29 μm QCLs working in continuous mode above 370 K with a CW output power as high as 312 mW at 300 K were obtained[29]. Next, narrow stripe-width, low-ridge MOCVD-grown QCLs emitting at 5.3 μm were fabricated, and a maximum peak-pulsed output power of 12 W at 14 A was measured[47]. Wang et al.[16] reported one low threshold MOCVD-grown QCL base on two-phonon resonance design. Continuous-wave operation threshold current density as low as 0.75 kA/cm^2, efficiency of 1079 mW/A, and total output power of 116 mW had been achieved at 288 K for a wavelength of 5.07 μm. Blaser et al. demonstrated one CW operating single mode QCL by
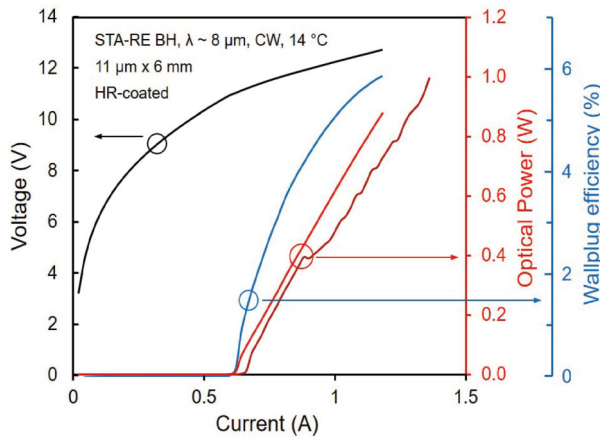
Fig. 17. (Color online) P–I–V and WPE of a 8.0 μm-emitting STA QCL under CW conditions measured at room temperature[24].

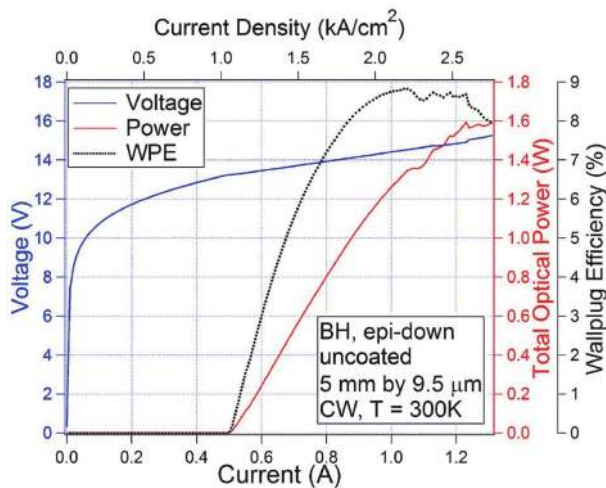Fig. 18. (Color online) P–I–V and WPE of a 9.5 μm × 5 mm long, HR-coated laser under CW conditions at 300 K[18].

MOCVD emitting at 5.25 μm with a threshold current of 75 mA and total power consumption of less than 2 W[48]. This considerably low thermal power dissipation made these devices very attractive for practical applications. These devices were the early research results of mid-infrared MOCVD-grown QCLs. Their emitting wavelengths were slightly longer than 5 μm and output powers were about several hundreds of milliwatts. Further research on material growth and active region design optimization was needed to adjust emitting wavelengths and increase output power.

For material growth, Wang *et al*. reported the growth and characterization of highly strain-compensated InGaAs/InAlAs/InP quantum-well heterostructures for mid-infrared QCLs[49, 50]. Growth conditions were established to provide a step-flow growth mode, which was important for precise thickness control of the ultrathin (~1 nm) epilayers of the active regions. For active region optimization, Lyakh *et al*. demonstrated 4.6 μm MOCVD-grown QCLs with optimized two-phonon resonance structure based on strain compensated $In_{0.67}Ga_{0.33}As/Al_{0.64}In_{0.36}As$ materials with highly strained (1%)[18]. A maximum total optical power of 1.6 W was obtained in CW mode at 300 K for uncoated devices fabricated in buried heterostructure geometry with stripe dimensions of 5 mm by 9.5 μm, as shown in Fig. 18. Corresponding

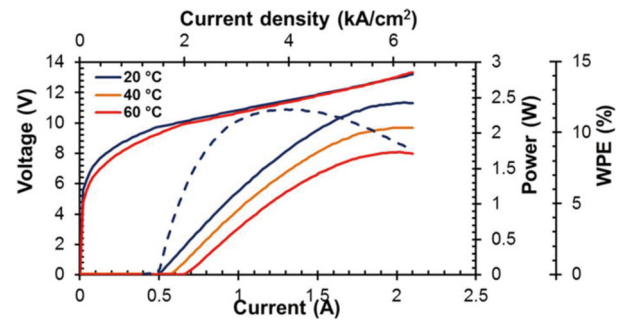Fig. 19. (Color online) P–I–V of a 5.5 μm × 6 mm long, HR-coated laser under CW conditions at different temperature. WPE (dash line) of a 5.5 μm × 6 mm long, HR-coated laser under CW conditions at 293 K[22].

maximum wall plug efficiency and threshold current density were measured to be 8.8% and 1.05 kA/cm², respectively. The FWHM of the electroluminescence (EL) of the laser grown by MBE is reduced by 20% compared with the laser grown by MOCVD, which directly affects the performance of the laser[18]. On the one hand, because differential gain is inversely proportional to line width, the differential gain will decrease. On the other hand, the larger line width simultaneously increases the non-harmonic oscillator interband loss and decreases the peak gain, both of which lead to higher laser threshold current density. At present, there is still a gap compared with the results of MBE. Then, high temperature CW operation of a distributed Bragg reflector (DBR) QCL based on MOCVD was demonstrated by Xie *et al*.[22]. They used a material system of $Ga_{0.22}In_{0.78}As/Al_{0.72}In_{0.28}As$, which had higher band shift, to further inhibit the thermal leakage of upper lasing level carriers. An output power of 2.5 W and a CW WPE of 11.7% were demonstrated for the FP device, as shown in Fig. 19. A CW output power of 2 W and a single mode operation with side mode suppression ratio of 30 dB around wavelength of 4.48 μm were achieved at 20 °C for the DBR device.

To further improve the device performance, a deep-well design was proposed by Botez. The authors systematically studied the theoretical design and material growth of this deep-well design using MOCVD. They grew InGaAs/GaAsP/AlGaAs strain-compensated deep-well QC structures by MOCVD. By lowering the growth temperature to 580 °C, high-quality X-ray spectra and resonant tunneling diode action were obtained from the $In_{0.4}Ga_{0.6}As/Al_{0.8}Ga_{0.2}As$ structures for QCL emission in the 4–5 μm range[53]. Next, they developed highly temperature insensitive 4.8 μm QCL that suppressed carrier leakage out of the active regions to the continuum states by using deep quantum wells, tall barriers, and tapered conduction-band-edge relaxation regions[52]. The calculated conduction-band (CB) profiles and key wave functions for conventional and deep-well designs are illustrated in Fig. 20. Tight confinement of injected carriers to the active wells was achieved, which in turn introduced the reduction of the threshold current density relative to conventional QC lasers. Next, they developed the step-taper active-region (STA) structure by taking advantage of flexibility of MOVPE for growth of SL structures composed of multiple alloy compositions. The STA structure has also demonstrated impressive results in the LWIR range, as mentioned above. In the mid-
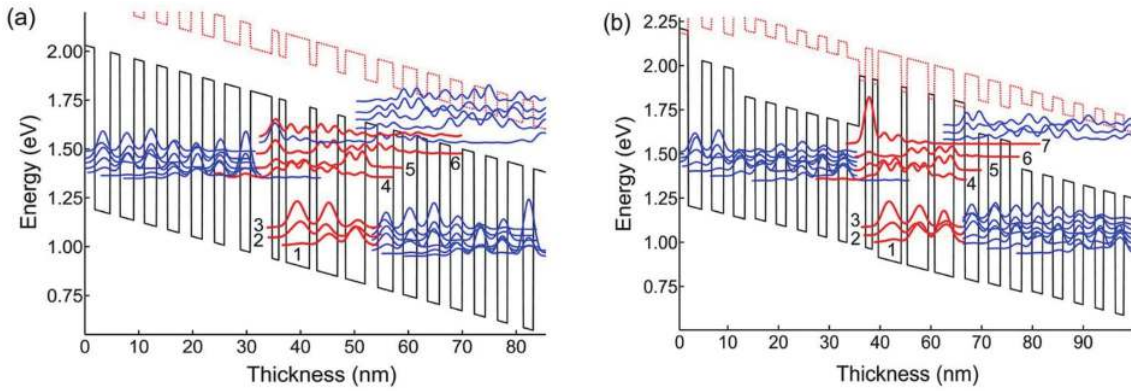
Fig. 20. (Color online) Calculated CB profile and key wave functions for (a) Conventional QC laser emitting at 4.8 μm[51]. (b) Deep-well QC laser under an electric field of 75 kV/cm ($\lambda \approx 4.8$ μm). The upper lasing level is labeled as 4, while 5, 6, and 7 are upper energy levels in the active region. The band profile at the top of each figure corresponds to the X valley[52].
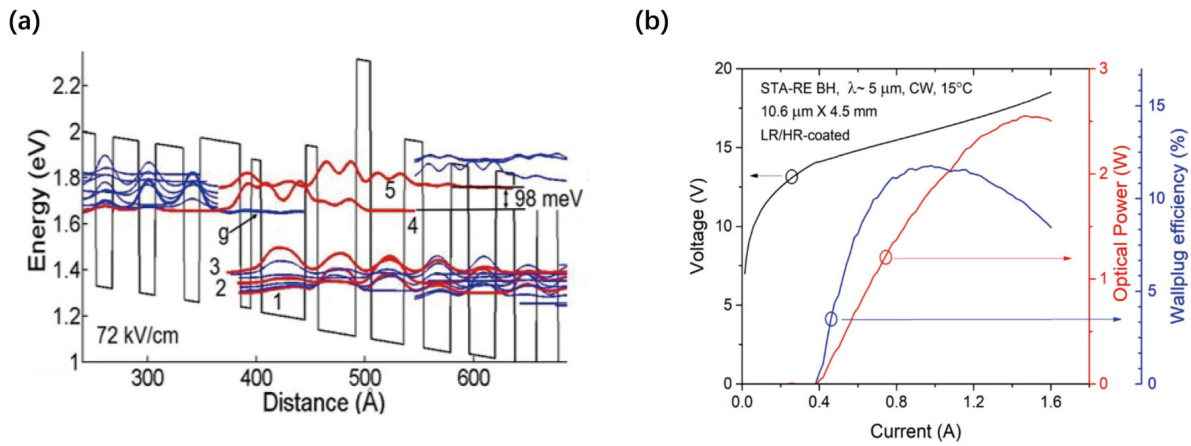

Fig. 21. (Color online) (a) A schematic diagram of the energy band under an electric field intensity of 72 kV/cm. (b) P−I−V and WPE of a 10.6 μm × 4 mm long, HR-coated laser under CW conditions at 300 K[24].
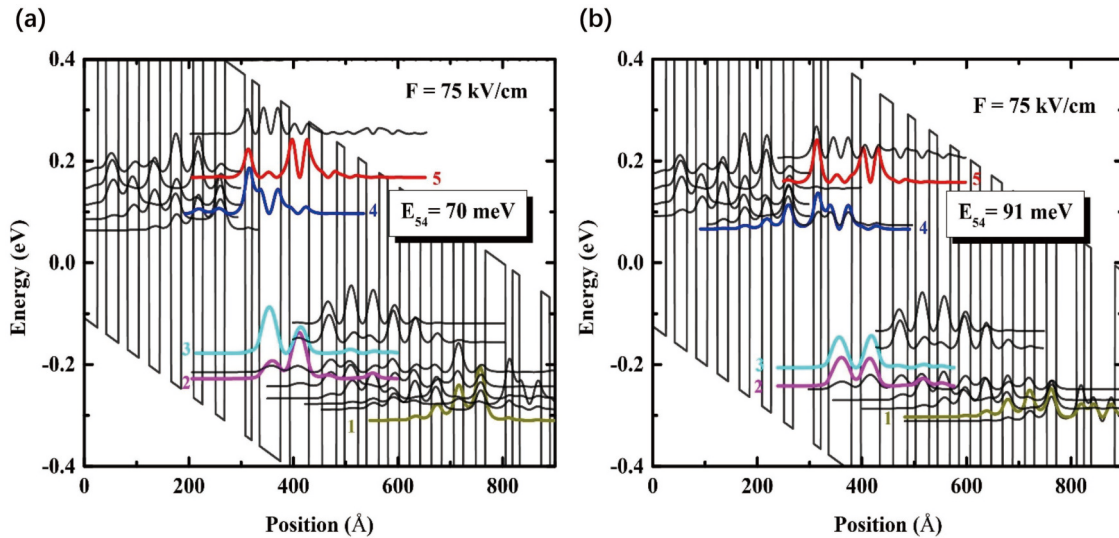

Fig. 22. (Color online) (a) Schematic diagram of the reference energy band at an electric field strength of 75 kV/cm. (b) Schematic diagram of the modified energy bands at an electric field strength of 75 kV/cm[55].

infrared range, the crystal growth of varying-layer-composition, 4.8 μm-emitting, tapered active-region (TA) QCLs were first demonstrated[54]. Transmission-electron-microscope analysis of the QCL structure confirmed extremely accurate thickness control and layer uniformity for layers as thin as 1 nm. A room temperature CW maximum power laser of 2.6 W and a

WPE of 12.5% were obtained at 5 μm[24] at 288 K based on the STA structure, as shown in Fig. 21. These results show the potential for performance improvement with superlattice (SL) structures composed of multiple alloy compositions.

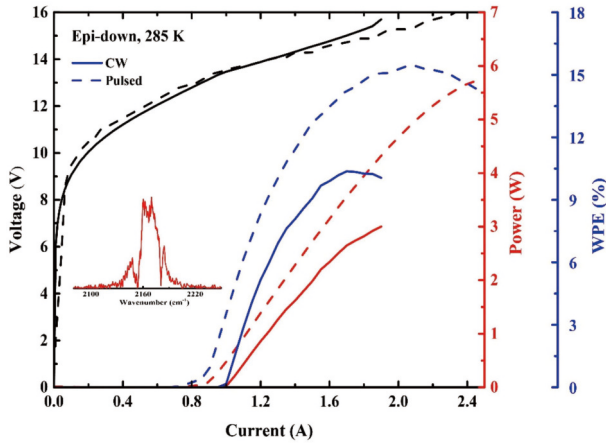In the subsequent development, Fei et al. reported the growth and fabrication of 4.6 μm strain-balanced

Fig. 23. (Color online) P–I–V and WPE of a 10.6 μm × 4 mm long, HR-coated laser under CW and pulsed conditions at 300 K[55].
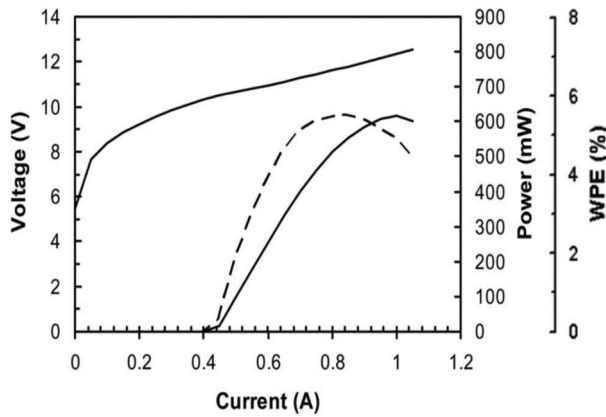

Fig. 24. (Color online) P–I–V and WPE curves of a 5 μm × 4 mm long emitting 4.0 μm laser with a 90% HR coating in CW mode at 288 K[21].

$In_{0.66}Ga_{0.34}As/In_{0.36}Al_{0.64}As$ using MOCVD. The laser core consisted of 40 periods of strain-balanced InGaAs/InAlAs quantum well and barrier pairs based on the single phonon resonance (SPR) design similar to the structure in Ref. [55]. Fig. 22 demonstrates a comparison between the design in the reference and the one optimized. The thickness of the active region was slightly modified to target the wavelength of 4.5 μm. In addition, the compositions of Al in InAlAs and Ga in InGaAs were changed to 0.64 and 0.34, respectively. Thus, the band offset was increased from 708 to 782 meV. Therefore, thermal leakage of electrons from the upper lasing level could be suppressed. Another notable feature was the increased energy separation between the upper lasing state E_4 and the excited state E_5. The calculated difference E_{54} was increased from 70 to 91 meV. Fig. 23 shows the CW (solid lines) and pulsed (dash lines) PIV and WPE results of this MOCVD-grown QCL at 285 K. The AR-HR coated device exhibited a CW output power of 3 W with threshold current density J_{th} = 1.76 kA/cm², slope efficiency 4 W/A, and WPE 10.4%.

The wavelength comfort zone for high power QCLs in the mid-infrared range is 4–5 μm, and high-power 3–4 μm QCLs are a difficult issue of QCL research. Due to the higher photon energies, it is necessary to increase the band offset to 1 eV or higher, which need to further increase the composition of Al in InAlAs and decrease the composition of Ga in InGaAs. This will induce larger material strain (in the range of

Table 2. The most notable research results across various wavelength ranges realized by MOCVD.

Classification	Authors	Wavelength (μm)	RT CW Power (W)	RT CW WPE (%)
Short-wavelength QCL (3−5 μm)	Xie et al.[21]	4.0	0.6	5.5
	Lyakh et al.[18]	4.6	1.6	8.8
	Xie et al.[22]	4.6	2.5	11.7
	Fei et al.[55]	4.6	3.0	10.4
	Botez et al.[24]	4.9	2.6	12.5
Long-wavelength QCL (8−12 μm)	Troccoli et al.[59]	7.5	0.8	3.4
	Wang et al.[39]	8.0	1	6
	Fei et al.[42]	8.5	1	7.1
	Troccoli et al.[59]	8.9	0.92	4
	Sun et al.[19]	9.0	1	5
	Wang et al.[23]	9.3	1.32	6.8
	Xie et al.[20]	10.7	1.3	4.4

1.3%–1.6%), which greatly increases the difficulty of material preparation. The high-performance laser with wavelength near 4 μm was first obtained by MBE[56]. Using MOCVD, Revin firstly reported the development of 4 μm highly strain-compensated $In_{0.7}Ga_{0.3}As/In_{0.34}Al_{0.66}As/InP$ QCLs. 10 μm-wide and 3 mm-long devices delivered more than 2.4 W peak power from both facets at 300 K, and operated up to about 400 K with characteristic temperature of 153 K. Then, Xie et al. demonstrated the evolution of short wavelength QCLs with strain balanced $Ga_xIn_{1−x}As/Al_yIn_{1−y}As$ starting from λ = 4.6 μm QCLs with modified two-phonon resonance designs. Benefiting from the combination of a proper design with deep QWs, high-quality growth, and good thermal managing, 4.0, 3.8, and 3.5 μm QCLs were realized. The CW output powers at 3.8 and 3.5 μm achieved up to 400 and 60 mW at room temperature, respectively. The CW P–I–V curves in Fig. 24 were measured for a submounted 4.0 μm QCL chip with a stripe width of 5 μm. As shown in Fig. 24, The output CW power was more than 600 mW, and the CW WPE reached 5.5%. The output power and WPE per unit active area were similar to those realized based on MBE by Lyakh et al.[57]. For low-strain designs, Mawst et al. proposed structures for short-wavelength (~3.6 μm) QCL employing a metamorphic buffer layer (MBL) on a GaAs substrate. The strain thickness product values for the quantum wells and barriers were kept basically the same as those employed for longer wavelength (~4.8 μm) QCL structures grown on InP substrates. Although inter subband absorption was observed for doped SL structures grown by MOCVD, further intense research was need for incorporation of such active regions into QCL-device structures[58]. Carrier leakage is an important factor limiting the performance of short-wavelength quantum cascade lasers (i.e. the parasitic energy level and continuous state in which electrons escape to the upper energy level). An effective method is to use large strain InGaAs and InAlAs quantum well pairs, and then increase the depth of the quantum well to inhibit carrier leakage. The second method is AlAs or InAs intercalation, which reduces the probability of carrier escaping to parasitic level and improves the injection efficiency. At the same time, the difficulty of epitaxial growth of short-wave quantum cascade laser is reduced, and the fault tolerance of material growth is improved.

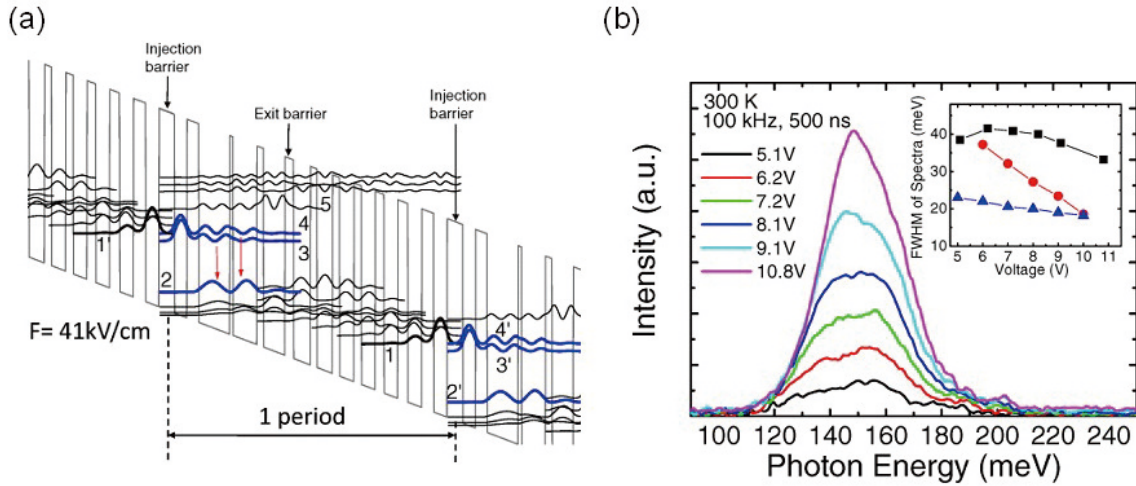**Y Q Sun et al.: Quantum cascade lasers grown by MOCVD**

Fig. 25. (Color online) (a) A schematic diagram of the energy band under an electric field intensity of 41 kV/cm. (b) EL spectrum curves between sub-bands of the mesa device at different voltages. The inset shows FWHM of the EL spectrum for the double upper level (solid squares), BTC (solid circles)[64], and bound to bound (solid triangles) as a function of voltage[61].
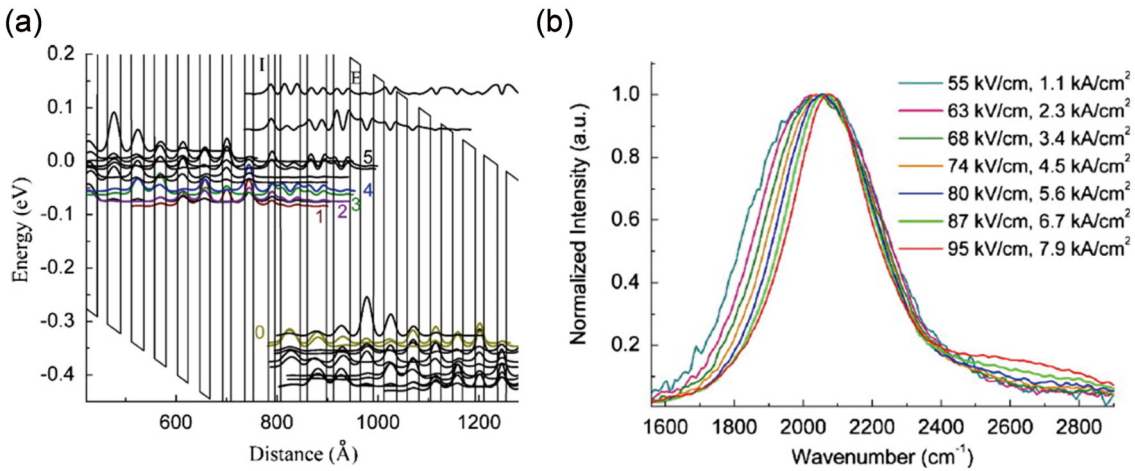

Fig. 26. (Color online) (a) Schematic diagram of the energy bands of the continuum-to-continuum designed active region structure under an electric field of 69 kV/cm. (b) EL spectra under different electric fields at a temperature of 295 K[65].

In order to visualize the current research progress of high power QCL, we summarize the most notable research results across various wavelength ranges in Table 2. Over the past 20 years, MOCVD-grown QCLs have obtained exciting progress and show tremendous potential at growing high performance devices.

4. MOCVD-grown broad gain spectrum QCL

Besides output power, spectral tunability is another important factor that is imperative in the application of infrared laser spectroscopy, such as gas sensing and medical diagnosis. For such applications, the tunning width, which is determined by the gain spectrum bandwidth, has become the limited factor. Therefore, research on wide gain QCLs has attracted much interest and great progress has been made based on MOCVD recently.

To broaden the gain spectral, the active region design of bound-to-continuum (BTC) structure, which was proposed and realized using MBE originally[60], is a good choice. This design could broad the gain spectrum by increasing the energy levels involved in the transitions. Inspired by BTC design, Fujita *et al.* proposed a dual-upper-state (DAU)[31, 43, 61−63]

device emitting at 8.4 μm using MOCVD, in which the upper lasing level split into two levels with a separation of 20−30 meV. The typical band structure is shown in Fig. 25(a). The upper lasing levels 4 and 3 had equal oscillator strengths for the transitions to the lower common lasing states in order to achieve a broad spectrum. The wave functions of these two upper levels extended throughout the whole active region from injection barrier to exit barrier, resulting in large transition matrix element of 1.8 nm[61]. Furthermore, the energy difference between the upper laser states and parasitic state 5 can be designed to be as large as 60 meV, which enabled the high injection efficiency for the both upper states even at high temperature. Therefore, this structure not only exhibited a broad gain spectrum but also demonstrated high temperature device characteristics. A bandwidth, which was evaluated through the EL FWHM, was measured to 40.8 meV (330 cm^{-1}) at the operating voltage of 7.2 V as shown in Fig. 25(b). The device exhibited high temperature stability with a T_0 value of 306 K and constant slope efficiency over the wide temperature range 280−400 K.

A MOCVD-grown device named continuum-to-continuum has been demonstrated, in which increasing number of
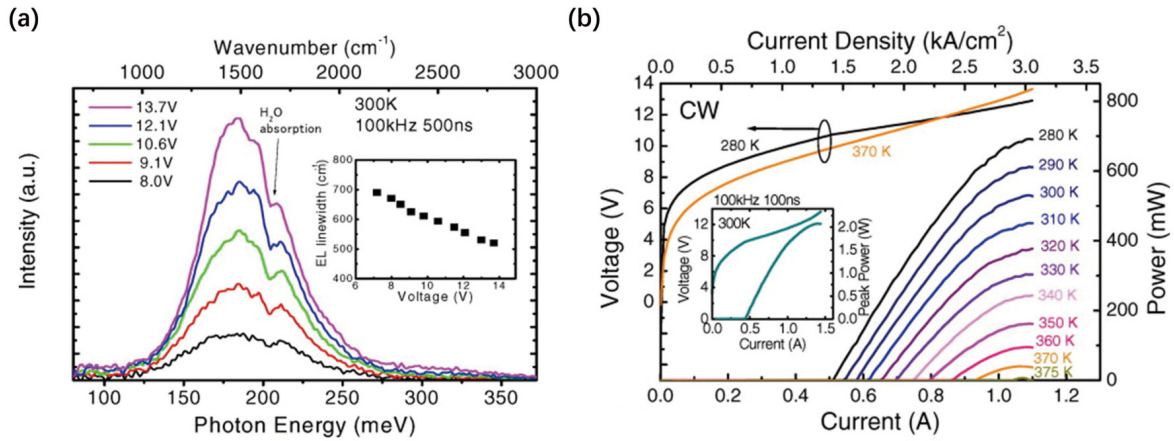
Fig. 27. (Color online) (a) EL spectra at different voltages at 300K. (b) *P–I* of a 12 *µm* × 3 mm long, HR-coated laser under CW conditions at different temperature. The voltage–current curves at 280 and 370 K are intentionally shown. *P– I–V* of a 12 *µm* × 3 mm long, HR-coated laser under pulsed conditions and 1% duty cycle at 300 K[62].
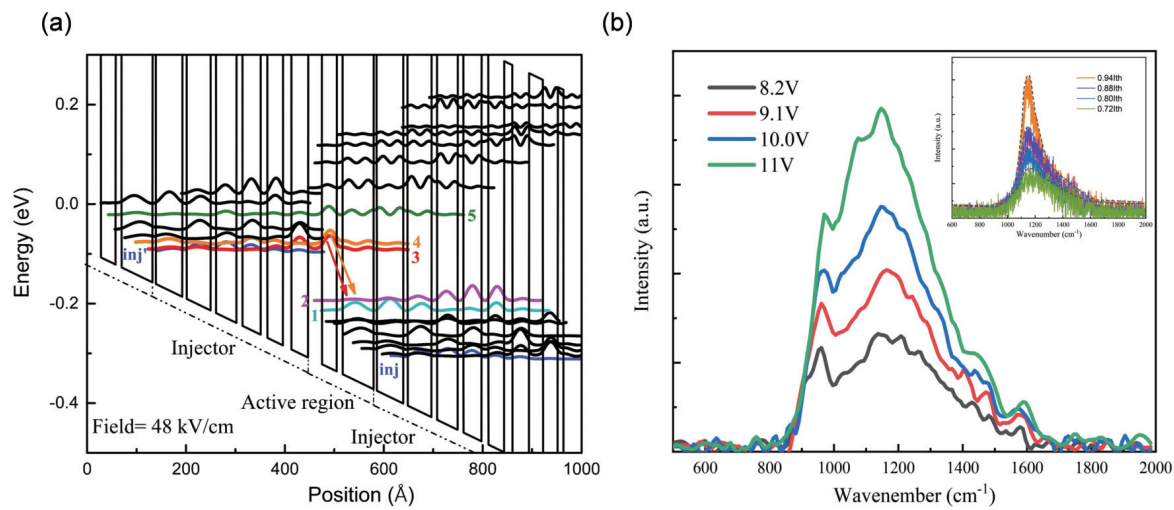

Fig. 28. (Color online) (a) A schematic diagram of the energy band under an electric field intensity of 48 kV/cm. (b) EL spectra of a 4 mm long, 10.5 *µm* wide, HR-coated, disrupted QCL burying the backside of the heterostructure. The inset shows the subthreshold amplified spontaneous emission spectrum of the device in pulsed mode at 300 K (80 kHz, 3 *µs*)[19].

upper lasing levels involved in the transitions were designed compared to BTC structure[65]. Fig. 26(a) illustrates the schematic conduction band diagram. Strong coupling of the three injector states with the upper lasing state resulted in their diffusion into the active region, and thus transitions from all these four levels could contribute to the gain spectrum. The strong coupling could not only provide more transition channels to broaden the gain spectral width but also enhance the injection rate from the injector state to the upper lasing state. Based on this design, a gain spectral width of 430 cm^{-1} around 4.8 *µm* was obtained, as shown in Fig. 26(b). In spite of the broad gain spectrum, high laser performance was demonstrated with low threshold current density of 1.6 kA/cm^2 and high wall plug efficiency up to 23% in pulsed mode at 295 K.

For broader gain spectrum, MOCVD-grown devices with extremely wide EL (600 cm^{-1}) around 6.8 *µm* were demonstrated based on the anticrossed DAU to multiple-lower-state (MS) design, as depicted in Fig. 27(a)[62]. As shown in Fig. 27(b), a high power of 500 mW with a high slope efficiency of 1.6 W/A in CW mode and a maximum CW operating temperature above 100 °C were achieved. Subsequently,

Fujita *et al.* has expand DAU scheme to the LWIR range (>10 *µm*)[66]. The DAU device demonstrated a CW lasing up to 300 K, with a low threshold current density of 2.1 kA/cm^2. The FWHM of the EL spectra was over 300 cm^{-1} for all voltage ranges. Furthermore, an external-cavity (EC) laser with tunable wavelength range from 9.5 to 11.4 *µm* (176 cm^{-1}, corresponding to 18% of the center wavelength) in CW operation at room temperature was obtained with this broad gain chip.

Although Fujita *et al.* have demonstrated a series of devices with broad gain spectral width based on MOCVD, the output power of these devices barely achieved watt level in CW operation mode. To increase output power, Sun *et al.* designed a 9 *µm* QCL with optimized DAU to MS design, as shown in Fig. 28(a)[19]. The double upper energy levels and the lower energy levels were designed diagonally to make the electrons of the upper energy levels highly localized to achieve higher efficiency of population inversion. Finally, a 4-mm-long cavity length and 10.5-*µm*-wide ridge MOCVD-grown QCL with high-reflection (HR) coating demonstrated a maximum CW output power of 1.02 W at 293 K. Meanwhile, due to the DAU design, this device exhibited a 466 cm^{-1} (57.8 meV) EL spectrum, as shown in Fig. 28(b).
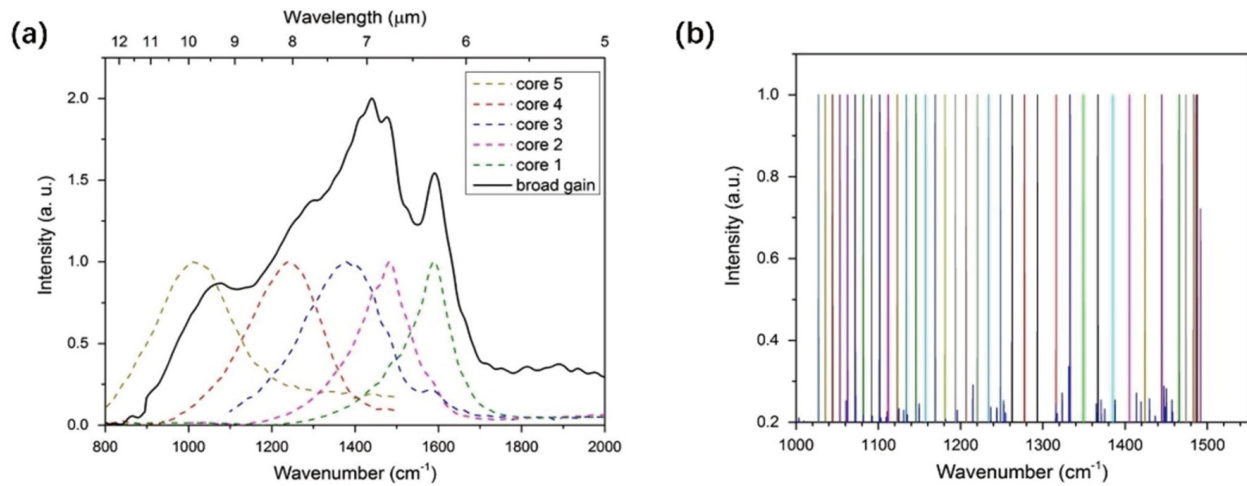
Fig. 29. (Color online) (a) Normalized mesa EL spectra of broad-gain wafers with each individual active region and multiple active regions. (b) 6.5 $\mu m \times$ 6 mm gain chip under pulsed external cavity tuning laser spectrum[71].

Another approach to broad the gain spectral is through integration of active regions of different wavelengths within one QCL, that is a multi-core heterogeneous structure. When designing a heterogeneous cascade structure, the total gain and spectral overlap of the gain curves of the individual stages are both important. This makes the carrier transition smoothly between the energy levels corresponding to different wavelengths. At the same time, the band level can be increased to prevent carrier leakage and improve performance.

EC-QCLs with multi-cores for different wavelength range have been realized based on MBE and a maximum tuning range from 5.2–11 μm has been obtained[67–70]. The growth of multi-core QCLs based on MOCVD was first reported by Xie et al. in 2015[71]. They grew five QC cores with gain peaks ranging from 6.3 to 9.9 μm across Core 1 through Core 5, as depicted in Fig. 29(a). To optimize the confinement factor of each core at corresponding wavelengths, these five QC cores are stacked roughly symmetrically with the shortest wavelength core in the central position and longest wavelength core in the outer positions. An ultrabroad gain profile that covered the wavelength range from 6.5 to 10.4 μm was obtained. In a grating-tuned external cavity QCL, they demonstrated continuous tuning from 1027 to 1492 cm^{-1}, as shown in Fig. 29(b). Furthermore, they also fabricated distributed feedback QCL arrays and single wavelength lasing from 962 cm^{-1} (10.4 μm) to 1542 cm^{-1} (6.5 μm) was obtained. These results demonstrate the ability of MOCVD to grow multicore devices. Actually, due to the growth stability and flexibility, MOCVD is more promising technique for growing multicore QCLs compared to MBE.

5. Future prospects of QCLs grown by MOCVD

As one of the most ideal mid-infrared semiconductor lasers, quantum cascade lasers have broad applications in infrared countermeasures, gas detection, free space communication and other fields. The large demand in the mid-infrared field is driving quantum cascade lasers increasingly toward the consumer market. In the past two decades, MOCVD-grown QCLs achieved great progress and show tremendous potential for high performance devices.

However, in terms of the highest performance metrics, for example the highest output power, there is still a gap compared with MBE-grown QCLs. To further improve device performance, future research should be fixed on active region optimization based on variable composition design, which will take full advantage of the growth flexibility of MOCVD and provide more design freedom. Based on the characteristics of multi-channel MO source, several components of InAlAs/InGaAs in the active region are designed and optimized. For example, the introduction of AlAs and InAs layers into the design of energy levels in the active region. The short-wavelength QCL is further extended to less than 3.5 μm and the LWIR QCL is increased to more than 11 μm. The expansion of laser wavelength is of great significance for more applications in service and daily production and life. A wide tuned laser with multiple active cores is used to achieve monolithic photon integration. This device is simple and portable, and designed to meet the needs of life. With the development of MOCVD technology, the performance of QCL based on MOCVD growth continues to improve. Due to the advantages of high efficiency, short maintenance cycles, and high stability and repeatability of MOCVD, this will greatly promote the mass production and application of QCL. The increasing demand for QCL advances the commercialization of QCL in future.

6. Conclusion

This overview provides a comparative summary of the recent progress of QCLs grown by MOCVD, focusing on the performance improvement of MOCVD-grown QCLs based on the optimizations of material quality and active region structure. Finally, the future of QCLs grown by MOCVD is prospected.

Acknowledgments

References

[1] Faist J, Capasso F, Sivco D L, et al. Quantum cascade laser. Science, 1994, 264, 553

[2] Curl R F, Capasso F, Gmachl C, et al. Quantum cascade lasers in chemical physics. Chem Phys Lett, 2010, 487, 1

[3] Liu X, Van Neste C W, Gupta M, et al. Standoff reflection–absorption spectra of surface adsorbed explosives measured with pulsed quantum cascade lasers. Sens Actuator B-Chem, 2014, 191, 450

[4] Wysocki G, Kosterev A A, Tittel F K. Spectroscopic trace-gas sensor with rapidly scanned wavelengths of a pulsed quantum cascade laser for *in situ* NO monitoring of industrial exhaust systems. Appl Phys B, 2005, 80, 617

[5] Zhang L Z, Tian G A, Li J S, et al. Applications of absorption spectroscopy using quantum cascade lasers. Appl Spectrosc, 2014, 68, 1095 [

[6] Liu J H, Wang H A, et al. Broad tuning range, high power quantum cascade laser at λ ~ 7.4 μm. Opt Express, 2022, 30, 40704

[7] Sun Y, Yang K, Liu J, et al. , High sensitivity and fast detection system for sensing of explosives and hazardous materials. Sens Actuator B-Chem, 2022, 360, 131640

[8] Schwaighofer A, Brandstetter M, Lendl B. Quantum cascade lasers (QCLs) in biomedical spectroscopy. Chem Soc Rev, 2017, 46, 5903

[9] Yao Y, Hoffman A J, Gmachl C F. Mid-infrared quantum cascade lasers. Nature Photon, 2012, 6, 432

[10] Corrigan P, Martini R, Whittaker E A, et al. Quantum cascade lasers and the Kruse model in free space optical communication. Opt Express, 2009, 17, 4355

[11] Zhuo N, Liu F Q, Wang Z G. Quantum cascade lasers: From sketch to mainstream in the mid and far infrared. J Semicond, 2020, 41, 010301

[12] Bai Y, Bandyopadhyay N, Tsao S, et al. Room temperature quantum cascade lasers with 27% wall plug efficiency. Appl Phys Lett, 2011, 98, 181102

[13] Roberts J S, Green R P, Wilson L R, et al. Quantum cascade lasers grown by metalorganic vapor phase epitaxy. Appl Phys Lett, 2003, 82, 4221

[14] Green R P, Krysa A, Roberts J S, et al. Room-temperature operation of InGaAs/AllnAs quantum cascade lasers grown by metalorganic vapor phase epitaxy. Appl Phys Lett, 2003, 83, 1921

[15] Diehl L, Bour D, Corzine S, et al. Pulsed- and continuous-mode operation at high temperature of strained quantum-cascade lasers grown by metalorganic vapor phase epitaxy. Appl Phys Lett, 2006, 88, 041102

[16] Wang X J, Fan J Y, Tanbun-Ek T, et al. Low threshold quantum-cascade lasers of room temperature continuous-wave operation grown by metal-organic chemical-vapor deposition. Appl Phys Lett, 2007, 90, 211103

[17] Evans A, Yu J S, David J, et al. High-temperature, high-power, continuous-wave operation of buried heterostructure quantum-cascade lasers. Appl Phys Lett, 2004, 84, 314

[18] Lyakh A, Pflügl C, Diehl L, et al. 1.6W high wall plug efficiency, continuous-wave room temperature quantum cascade laser emitting at 4.6μm. Appl Phys Lett, 2008, 92, 201103

[19] Sun Y Q, Yin R, Zhang J C, et al. High-performance quantum cascade lasers at λ ~ 9 μm grown by MOCVD. Opt Express, 2022, 30, 37272

[20] Xie F, Caneau C, Leblanc H P, et al. Watt-level room temperature continuous-wave operation of quantum cascade lasers with λ >10 μm. IEEE J Sel Top Quantum Electron, 2013, 19, 1200407

[21] Xie F, Caneau C, LeBlanc H P, et al. Room temperature CW operation of short wavelength quantum cascade lasers made of strain balanced Ga$_x$In$_{1-x}$As/Al$_y$In$_{1-y}$As material on InP substrates. IEEE J Sel Top Quantum Electron, 2011, 17, 1445

[22] Xie F, Caneau C G, LeBlanc H P, et al. High power and high temperature continuous-wave operation of distributed Bragg reflector quantum cascade lasers. Appl Phys Lett, 2014, 104, 071109

[23] Wang C A, Schwarz B, Siriani D F, et al. MOVPE growth of LWIR AllnAs/GaInAs/InP quantum cascade lasers: Impact of growth and material quality on laser performance. IEEE J Sel Top Quantum Electron, 2017, 23, 1

[24] Botez D, Kirch J D, Boyle C, et al. High-efficiency, high-power mid-infrared quantum cascade lasers [Invited]. Opt Mater Express, 2018, 8, 1378

[25] Botez D, Chang C C, Mawst L J. Temperature sensitivity of the electro-optical characteristics for mid-infrared (λ = 3–16μm)-emitting quantum cascade lasers. J Phys D: Appl Phys, 2016, 49, 043001

[26] Troccoli M, Bour D, Corzine S, et al. Low-threshold continuous-wave operation of quantum-cascade lasers grown by metalorganic vapor phase epitaxy. Appl Phys Lett, 2004, 85, 5842

[27] Krysa A B, Roberts J S, Green R P, et al. MOVPE-grown quantum cascade lasers operating at ~9μm wavelength. J Cryst Growth, 2004, 272, 682

[28] Troccoli M, Corzine S, Bour D, et al. Room temperature continuous-wave operation of quantum-cascade lasers grown by metal organic vapour phase epitaxy. Electron Lett, 2005, 41, 1059

[29] Diehl L, Bour D, Corzine S, et al. High-temperature continuous wave operation of strain-balanced quantum cascade lasers grown by metal organic vapor-phase epitaxy. Appl Phys Lett, 2006, 89, 081101

[30] Fujita K, Furuta S, Sugiyama A, et al. Room temperature, continuous-wave operation of quantum cascade lasers with single phonon resonance-continuum depopulation structures grown by metal organic vapor-phase epitaxy. Appl Phys Lett, 2007, 91, 141121

[31] Fujita K, Furuta S, Sugiyama A, et al. High-performance λ~8.6 μm quantum cascade lasers with single phonon-continuum depopulation structures. IEEE J Quantum Electron, 2010, 46, 683

[32] Pflügl C, Diehl L, Tsekoun A, et al. Room-temperature continuous-wave operation of long wavelength (λ=9.5 μm) MOVPE-grown quantum cascade lasers. Electron Lett, 2007, 43, 1026

[33] Huang Y, Ryou J H, Dupuis R D, et al. Optimization of growth conditions for InGaAs/InAlAs/InP quantum cascade lasers by metal-organic chemical vapor deposition. J Cryst Growth, 2011, 316, 75

[34] Demir I, Elagoz S. Interruption time effects on InGaAs/InAlAs superlattices of quantum cascade laser structures grown by MOCVD. Superlattices Microstruct, 2016, 100, 723

[35] Demir I, Elagoz S. V/III ratio effects on high quality InAlAs for quantum cascade laser structures. Superlattices Microstruct, 2017, 104, 140

[36] Wang C A, Goyal A K, Menzel S, et al. High power (>5 W) λ~9.6 μm tapered quantum cascade lasers grown by OMVPE. J Cryst Growth, 2013, 370, 212

[37] Wang C A, Schwarz B, Siriani D F, et al. Sensitivity of heterointerfaces on emission wavelength of quantum cascade lasers. J Cryst Growth, 2017, 464, 215

[38] Kelly T F, Miller M K. Invited review article: Atom probe tomography. Rev Sci Instrum, 2007, 78, 031101

[39] Schwarz B, Wang C A, Missaggia L, et al. Watt-level continuous-wave emission from a bifunctional quantum cascade laser/detector. ACS Photonics, 2017, 4, 1225

[40] Molodtsov I S, Raspopov N A, Lobintsov A V, et al. Quantum cascade laser with bound-to-quasi-continuum optical transitions at a temperature of up to 371 K. Quantum Electron, 2020, 50, 710

[41] Fan J A, Belkin M A, Troccoli M, et al. Double-metal waveguide ≃19 μm quantum cascade lasers grown by metal organic vapour phase epitaxy. Electron Lett, 2007, 43, 1284

[42] Fei T, Zhai S Q, Zhang J C, et al. High power λ ~ 8.5 μm quantum cascade laser grown by MOCVD operating continuous-wave up to 408 K. J Semicond, 2021, 42, 112301

[43] Fujita K, Yamanishi M, Furuta S, et al. Extremely temperature-insensitive continuous-wave quantum cascade lasers. Appl Phys Lett, 2012, 101, 181111

[44] Kirch J D, Shin J C, Chang C C, et al. Tapered active-region quantum cascade lasers (λ=4.8 μm) for virtual suppression of carrier-leakage currents. Electron Lett, 2012, 48, 234

[45] Liu Z J, Wasserman D, Howard S S, et al. Room-temperature continuous-wave quantum cascade lasers grown by MOCVD without lateral regrowth. IEEE Photonics Technol Lett, 2006, 18, 1347

[46] Kirch J D, Chang C C, Boyle C, et al. 86% internal differential efficiency from 8 to 9 μm-emitting, step-taper active-region quantum cascade lasers. Opt Express, 2016, 24, 24483

[47] Lyakh A, Zory P, Wasserman D, et al. Narrow stripe-width, low-ridge high power quantum cascade lasers. Appl Phys Lett, 2007, 90, 141107

[48] Blaser S, Bächle A, Jochum S, et al. Low-consumption (below 2 W) continuous-wave singlemode quantum-cascade lasers grown by metal-organic vapour-phase epitaxy. Electron Lett, 2007, 43, 1201

[49] Wang C A, Huang R K, Goyal A, et al. OMVPE growth of highly strain-balanced GaInAs/AlInAs/InP for quantum cascade lasers. J Cryst Growth, 2008, 310, 5191

[50] Wang C A, Goyal A, Huang R, et al. Strain-compensated GaInAs/AlInAs/InP quantum cascade laser materials. J Cryst Growth, 2010, 312, 1157

[51] Evans A, Yu J S, Slivken S, et al. Continuous-wave operation of λ~4.8μm quantum-cascade lasersat room temperature. Appl Phys Lett, 2004, 85, 2166

[52] Shin J C, D'Souza M, Liu Z, et al. Highly temperature insensitive, deep-well 4.8 μm emitting quantum cascade semiconductor lasers. Appl Phys Lett, 2009, 94, 201103

[53] Xu D P, D'Souza M, Shin J C, et al. InGaAs/GaAsP/AlGaAs, deep-well, quantum-cascade light-emitting structures grown by metal-organic chemical vapor deposition. J Cryst Growth, 2008, 310, 2370

[54] Shin J C, Mawst L J, Botez D. Crystal growth via metal-organic vapor phase epitaxy of quantum-cascade-laser structures composed of multiple alloy compositions. J Cryst Growth, 2012, 357, 15

[55] Fei T, Zhai S Q, Zhang J C, et al. 3 W continuous-wave room temperature quantum cascade laser grown by metal-organic chemical vapor deposition. Photonics, 2023, 10, 47

[56] Bandyopadhyay N, Slivken S, Bai Y, et al. High power, continuous wave, room temperature operation of λ ~ 3.4 μm and λ ~ 3.55 μm InP-based quantum cascade lasers. Appl Phys Lett, 2012, 100, 212104

[57] Lyakh A, Maulini R, Tsekoun A, et al. High-performance continuous-wave room temperature 4.0-μm quantum cascade lasers with single-facet optical emission exceeding 2 W. Proc Natl Acad Sci USA, 2010, 107, 18799

[58] Mawst L J, Kirch J D, Chang C C, et al. InGaAs/AlInAs strain-compensated Superlattices grown on metamorphic buffer layers for low-strain, 3.6 μm-emitting quantum-cascade-laser active regions. J Cryst Growth, 2013, 370, 230

[59] Troccoli M, Lyakh A, Fan J, et al. Long-wave IR quantum cascade lasers for emission in the λ = 8-12μm spectral region. Opt Mater Express, 2013, 3, 1546

[60] Faist J, Beck M, Aellen T, et al. Quantum-cascade lasers based on a bound-to-continuum transition. Appl Phys Lett, 2001, 78, 147

[61] Fujita K, Edamura T, Furuta S, et al. High-performance, homogeneous broad-gain quantum cascade lasers based on dual-upper-state design. Appl Phys Lett, 2010, 96, 241107

[62] Fujita K, Furuta S, Sugiyama A, et al. High-performance quantum cascade lasers with wide electroluminescence (~600 cm^{-1}), operating in continuous-wave above 100 ℃. Appl Phys Lett, 2011, 98, 231102

[63] Fujita K, Furuta S, Dougakiuchi T, et al. Broad-gain (Δλ/λ$_0$~04), temperature-insensitive (T$_0$~510K) quantum cascade lasers. Opt Express, 2011, 19, 2694

[64] Wittmann A, Bonetti Y, Faist J, et al. Intersubband linewidths in quantum cascade laser designs. Appl Phys Lett, 2008, 93, 141103

[65] Yao Y, Wang X J, Fan J Y, et al. High performance "continuum-to-continuum" quantum cascade lasers with a broad gain bandwidth of over 400 cm^{-1}. Appl Phys Lett, 2010, 97, 081115

[66] Dougakiuchi T, Fujita K, Sugiyama A, et al. Broadband tuning of continuous wave quantum cascade lasers in long wavelength (> 10μm) range. Opt Express, 2014, 22, 19930

[67] Hugi A, Terazzi R, Bonetti Y, et al. External cavity quantum cascade laser tunable from 7.6 to 11.4 μm. Appl Phys Lett, 2009, 95, 061103

[68] Maulini R, Mohan A R, Giovannini M, et al. External cavity quantum-cascade laser tunable from 8.2 to10.4μm using a gain element with a heterogeneous cascade. Appl Phys Lett, 2006, 88, 201113

[69] Bandyopadhyay N, Bai Y, Slivken S, et al. High power operation of λ ~ 5.2–11 μm strain balanced quantum cascade lasers based on the same material composition. Appl Phys Lett, 2014, 105, 201113

[70] Bandyopadhyay N, Chen M, Sengupta S, et al. Ultra-broadband quantum cascade laser, tunable over 760 cm^{-1}, with balanced gain. Opt Express, 2015, 23, 21159

[71] Xie F, Caneau C, Leblanc H, et al. Ultra-broad gain quantum cascade lasers tunable from 65 to 104 μm. Opt Lett, 2015, 40, 4158

Yongqiang Sun received his Ph.D. from the Key Laboratory of Semiconductor Materials, Institute of Semiconductors, Chinese Academy of Sciences. He is mainly interested in mid-infrared quantum cascade laser material epitaxial growth, and device and application research.

Zhang Jinchuan is a researcher and doctoral supervisor at the Institute of Semiconductors, Chinese Academy of Sciences. He is a distinguished member of the Youth Promotion Association of the Chinese Academy of Sciences, and is currently the leader of the research group of low-dimensional structural materials and devices. He is mainly engaged in research on quantum cascade laser physics, technology, and testing. He has presided over more than 10 scientific research projects, including key research and development projects, projects of the National Natural Science Foundation of China, projects of the Youth Promotion Association of the Chinese Academy of Sciences, and projects of the Beijing Natural Science Foundation of China.

Zhai Shenqiang is a researcher at the Institute of Semiconductors, Chinese Academy of Sciences, and a member of the Youth Promotion Association of the Chinese Academy of Sciences. In 2022, he received funding from Excellent Young Scientists Fund of the National Natural Science Foundation of China. He has been engaged in material epitaxial growth, device physics, and application research of mid-to-far infrared semiconductor quantum cascade lasers for a long time. The bottleneck of the poor interface quality of MOCVD-grown QCL materials is broken by design innovation of the energy band structure of the active region and optimization of the growth scheme. Promoting QCL technology towards industrial application is of great significance.